Experimental Investigation of the Nature of the Magnetoresistance Effects in Pd-YIG Hybrid Structures

Tao Lin, Chi Tang, Hamad M. Alyahayaei, and Jing Shi
Department of Physics and Astronomy, University of California, Riverside, California 92521, USA
(Received 27 January 2014; published 18 July 2014)

In bilayers consisting of Pd and yttrium iron garnet ($Y_3Fe_5O_{12}$ or YIG), we observe vanishingly small room-temperature conventional anisotropic magnetoresistance but large new magnetoresistance that is similar to the spin Hall magnetoresistance previously reported in Pt-YIG bilayers. We report a temperature dependence study of the two magnetoresistance effects in Pt-YIG bilayers. As the temperature is decreased, the new magnetoresistance shows a peak, whereas the anisotropic magnetoresistance effect starts to appear and increases monotonically. We find that the magnetoresistance peak shifts to lower temperatures in thicker Pd samples, a feature characteristic of the spin current effect. The distinct temperature dependence reveals fundamentally different mechanisms responsible for the two effects in such hybrid structures.

DOI: 10.1103/PhysRevLett.113.037203 PACS numbers: 75.76.+j, 73.50.Jt, 75.40.Gb

The hybrid structures of a strong spin-orbit coupling (SOC) metal such as Pt and a magnetic insulator such as yttrium iron garnet (YIG) exhibit a variety of interesting spin current related phenomena such as spin pumping [1–3], the spin Seebeck effect (SSE) [4,5] and the spin Hall magnetoresistance (SMR) [6–8]. In all these structures, the SOC metal plays a role of the spin current detector based on the inverse spin Hall effect (ISHE). In SMR, the SOC metal also serves as a spin current generator. According to the SMR mechanism [7], the spin current generated by the spin Hall effect in the SOC metal is reflected from the interface, and then converted into a charge voltage by the SOC metal. In a sweeping in-plane magnetic field, SMR behaves like the conventional anisotropic magnetoresistance (AMR) in ferromagnetic conductors [9], a phenomenon arising from a completely different origin. SMR is a pure spin current phenomenon in such bilayer structures; whereas AMR can only originate from the proximity-effect-induced ferromagnetism in the SOC metal at the interface [10,11]. In reality, both possibilities may be present but may not be revealed at room temperature.

By setting the magnetization of YIG to different orientations, one can determine the anisotropic resistivities in all three orthogonal directions of the SOC metal, i.e. longitudinal $\rho_{\parallel}$, transverse ρ_T, and perpendicular $\rho_{\perp}$resistivities, where $\rho_{\parallel}$ represents the resistivity when the magnetization $\boldsymbol{M}$ is parallel to the current direction, and both ρ_T and $\rho_{\perp}$ are the resistivities when $\boldsymbol{M}$ is perpendicular to the current direction, but for the former, $\boldsymbol{M}$ lies in the film plane and for the latter $\boldsymbol{M}$ is perpendicular to the plane. In ferromagnetic metals, it is often found $\rho_{\parallel} > \rho_T \approx \rho_{\perp}$, which is the conventional AMR. However, in Pt-YIG bilayers, it was found that $\rho_{\parallel} \approx \rho_T \neq \rho_{\perp}$ at room temperature [7,12], a property not consistent with AMR. This raises a question about the nature of this room-temperature magnetoresistance effect.

Motivated by the recent room-temperature studies on Pt-YIG systems, we choose to study the temperature dependence of the anisotropic resistivities in Pt-YIG hybrid structures since we believe that it can reveal important distinctions between these the AMR and SMR effects as will be discussed below. First of all, Pd is known to have larger magnetic susceptibility than other $4d$ and $5d$ nonmagnetic transition metals [13]; therefore, it has a stronger tendency than other metals to have an induced ferromagnetic moment at the interface. Additionally, both SMR and AMR effects are interface phenomena; consequently, they critically depend on the quality of the interface and SOC metals. For example, since the SMR effect vanishes as the SOC metal thickness exceeds the spin diffusion length λ (i.e., $\sim$1.5 nm for Pt at room temperature [14,15]), the thickness variation of the SOC metal needs to be much smaller than this length scale. We have demonstrated the epitaxial growth of atomically flat YIG films with our pulsed laser deposition (PLD) as well as the deposition of a smooth Pd layer down to 1.5 nm with sputtering [16] which are suitable for this investigation. Furthermore, for chosen Pd thicknesses, we vary the sample temperature so that λ can be tuned continuously across the sample thickness and the effect of spin current is revealed. In addition, if the proximity induced ferromagnetism exists in SOC metals, the AMR effect becomes more pronounced at lower temperatures. AMR originates from different scattering rates between the current parallel to and perpendicular to the magnetization or the ferromagnetic spin directions. At high temperatures, the spin-dependent effect is diluted by spin-independent scattering events such as electron-phonon scattering. Hence, we expect the AMR effect to appear and increase monotonically as the temperatures is decreased.

Epitaxial and atomically flat YIG films are grown on gadolinium gallium garnet or GGG (110) substrates using PLD [16]. In this work, the thickness range of YIG films is

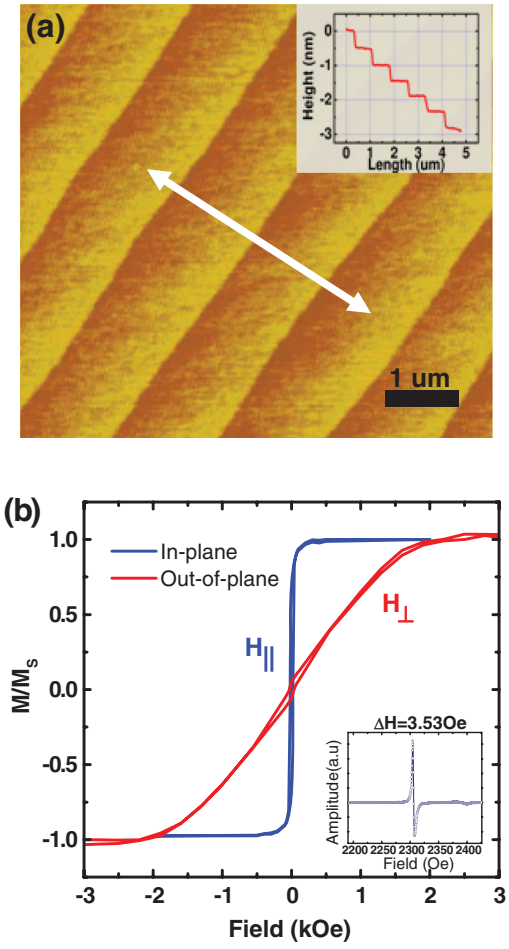

FIG. 1 (color). (a) AFM image of a representative YIG thin film. Inset: Line scan across the terraces (along the arrow direction). (b) Normalized magnetic hysteresis loops at 300 K of a YIG-GGG film with an applied field in-plane ($H_{\|}$) and out-of-plane ($H_{\perp}$). Inset: FMR spectrum of a bare 30 nm thick YIG on GGG.

from 16 to 50 nm. Figure 1(a) is an atomic force microscopy (AFM) image of a 30 nm thick YIG film. Flat terraces with a step height of 4.38 Å are present, indicating atomic steps between adjacent (110) planes. Magnetization measurements with the magnetic field oriented in both in-plane and out-of-plane directions reveal well-defined in-plane magnetic anisotropy [Fig. 1(b)]. The inset of Fig. 1(b) shows a typical ferromagnetic resonance (FMR) spectrum of a YIG film. The FMR linewidth is as narrow as $\Delta H = 3.53$ Oe and $4\pi M_s$ (M_s being the high saturation magnetization of YIG) ranges from 2000 to 2480 G, indicating excellent quality of YIG.

To prepare hybrid structures, YIG and GGG films are transferred to a high-vacuum sputtering chamber for metal deposition. A thin polycrystalline layer of Pd with a thickness range from 2 to 10 nm is deposited with magnetron sputtering after light sputter cleaning of the YIG surface. A thin MgO layer is then deposited on top to prevent oxidation. The Pd films are patterned into Hall bars oriented in two orthogonal directions with the bar width of 100 μm and length of 1,000 μm. The transport results from the two orthogonally oriented Pd Hall bars do not show any measurable difference, which is consistent with the polycrystalline nature of the Pd films. Magneto-transport measurements are performed in QUANTUM DESIGN's physical property measurement system with a rotating stage over a temperature range between 2 to 300 K.

Magnetoresistance of a Pd(2 nm)-YIG bilayer in an in-plane magnetic field shows low-field peaks (dips) located at the coercive fields of YIG [16]. This feature is similar to the AMR effect in polycrystalline ferromagnetic materials, but an alternative possibility is SMR. According to the SMR theory [6], a charge current flowing along the x direction as shown in Fig. 2(a) generates a y-polarized spin current, $\boldsymbol{j}_s$, flowing along the z direction. Depending on the orientation of $\boldsymbol{M}$ with respect to the spin direction of $\boldsymbol{j}_s$, the reflected spin current varies in magnitude, which yields an additional ISHE voltage superimposed on the longitudinal voltage signal. It has been shown [6,7] that the resulting SMR is

$$\frac{\Delta\rho}{\rho} \sim \frac{\Delta\rho_1}{\rho}(1 - m_y^2), \tag{1}$$

$$\frac{\Delta\rho_1}{\rho} = \theta_{\mathrm{SH}}^2 \frac{\lambda}{d} \frac{2\lambda G_r \tanh^2(\frac{d}{2\lambda})}{\sigma + 2\lambda G_r \coth(\frac{d}{2\lambda})}, \tag{2}$$

where m_y is the y component of the magnetization unit vector, and $\Delta\rho_1/\rho$ depends on λ, metal film thickness d, electrical conductivity of the metal film σ, spin Hall angle θ_{SH}, and the real part of the spin-mixing conductance G_r, as shown in Eq. (2). Clearly, the in-plane field sweep cannot distinguish AMR from SMR since both depend on the orientation of $\boldsymbol{M}$ in the xy plane. By rotating $\boldsymbol{M}$ in specific planes, however, it is possible to distinguish these two effects. As shown in Fig. 2(a), if $\boldsymbol{M}$ is rotated in the xz plane tracked by angle α, SMR should remain constant, since m_y, and therefore the reflection of $\boldsymbol{j}_s$, is unchanged; any resistance change can be attributed to AMR. On the other hand, if $\boldsymbol{M}$ is rotated in the yz plane tracked by angle β, AMR should remain constant, since the charge current is always perpendicular to $\boldsymbol{M}$; any resistance change can be attributed to SMR. In these two cases, magnetoresistance reveals different physical mechanisms. If $\boldsymbol{M}$ is rotated in the xy plane tracked by angle γ; however, both SMR and AMR change simultaneously and therefore the two effects are entangled.

Since the out-of-plane saturation field of YIG is $\sim$2 kOe, a magnetic field of 10 kOe is sufficiently strong to align and rotate the YIG magnetization $\boldsymbol{M}$ in any direction. Figure 2(b) shows a comparison of the relative changes of measured resistivity, $\Delta\rho/\rho_0$, at 100 and 3 K as a 10 kOe magnetic field is rotated in three orthogonal planes. For the α and β sweeps, 90° is chosen as the reference angle

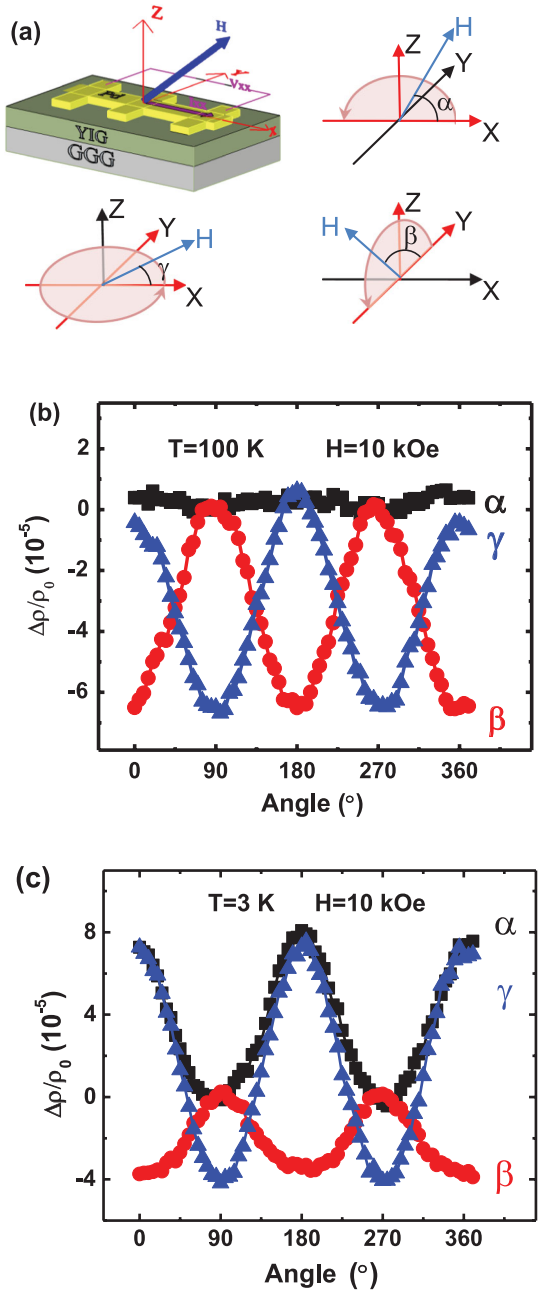

FIG. 2 (color). (a) Schematic diagram of the patterned Hall bar and notations for different field rotations. (b) and (c) show typical field rotation magnetoresistance data with H = 10 kOe in three orthogonal planes for Pd(2 nm)-YIG(30 nm) at 100 K (b) and 3 K (c).

for calculating $\Delta\rho$, i.e. $\Delta\rho = \rho(\alpha) - \rho(\alpha = 90°)$, and $\Delta\rho = \rho(\beta) - \rho(\beta = 90°)$, since $\alpha = 90°$ and $\beta = 90°$ coincide. For the γ sweep, 0° is chosen as the reference. ρ_0 is the resistivity at zero magnetic field. In all sweeps, the resistivity is a periodic function of the rotating angle with a period of 180°. To eliminate any mixed Hall signal that has a period of 360° due to any possible accidental misalignment of the longitudinal resistivity electrodes, we have removed a small background signal with a period of 360°. This background accounts for less than 10% of the total signal in the worst cases. At 100 K, the α sweep only shows very small amplitude, indicating a negligible AMR effect, i.e. $\rho_\parallel = \rho_\perp$. The amplitude of the γ sweep (~6%) corresponds well to that of the β sweep except that they are out of phase from each other. This is expected from Eq. (1) because the same m_y change is responsible for the SMR in the β sweep as well as the AMR in the γ sweep. At 3 K, all three sweeps register large amplitudes. This is in stark contrast with the room temperature or 100 K data which shows a nearly vanishing AMR effect. We also note that the amplitude of the β sweep is smaller than that at 100 K, indicating a nonmonotonic trend. The comparison at these two temperatures suggests different temperature dependence between SMR and AMR.

To find the detailed temperature dependence of these two effects, we have carried out the measurements over a range of temperatures on this 2 nm Pd sample. Figures 3(a), 3(b), and 3(c) show the anisotropic resistivities in all three sweeps. At all temperatures, $\Delta\rho/\rho_0$ oscillations can be well described by

$$\frac{\Delta\rho}{\rho_0} = \frac{\rho_\parallel - \rho_\perp}{\rho_0}\cos^2\alpha, \quad \frac{\Delta\rho}{\rho_0} = -\frac{\rho_\perp - \rho_T}{\rho_0}\cos^2\beta,$$
$$\frac{\Delta\rho}{\rho_0} = -\frac{\rho_\perp - \rho_T}{\rho_0}\cos^2\beta, \text{ and } \frac{\Delta\rho}{\rho_0} = \frac{\rho_\parallel - \rho_T}{\rho_0}\cos^2\gamma. \quad (3)$$

From those data, we immediately have $\rho_\parallel > \rho > \rho_T$ at low temperatures. Figure 3(d) plots the temperature dependence of the resistance oscillation amplitude for all three sweeps. Clearly, the α and β sweeps have distinctly different temperature dependences. Above a certain temperature (~100 K), the amplitude of the α sweep or AMR is negligibly small. As the temperature is decreased to below 100 K, AMR starts to appear and increases steadily. On the contrary, the amplitude of the β sweep or SMR has a peak at ~100 K. The overall temperature dependence of SMR is expected from the SMR theory as will be discussed below. From Eq. (3), it is clear that the amplitude of the γ sweep should be just the sum of those of the α and β sweeps if $\boldsymbol{M}$ rotates as a single-domain magnetization. Indeed, the sum calculated from the two temperature-dependent amplitudes of the α and β sweeps agrees well with the amplitude of the γ sweep measured separately, as shown in Fig. 3(d).

The unique peak in the β sweep is consistent with the SMR theory prediction [6]. In Eq. (2), the magnitude of SMR depends on the d/λ ratio. As the temperature is decreased, the spin Hall angle, the electrical conductivity, and the spin mixing conductivity of Pd will likely change somewhat, but we do not expect that they change significantly or in a nonmonotonic way. On the other hand, d/λ can change over a large range as the temperature is varied, which causes the right-hand side of Eq. (2) to change nonmonotonically. In fact, if we assume that SMR is a function of d/λ, as it varies, a SMR peak occurs at

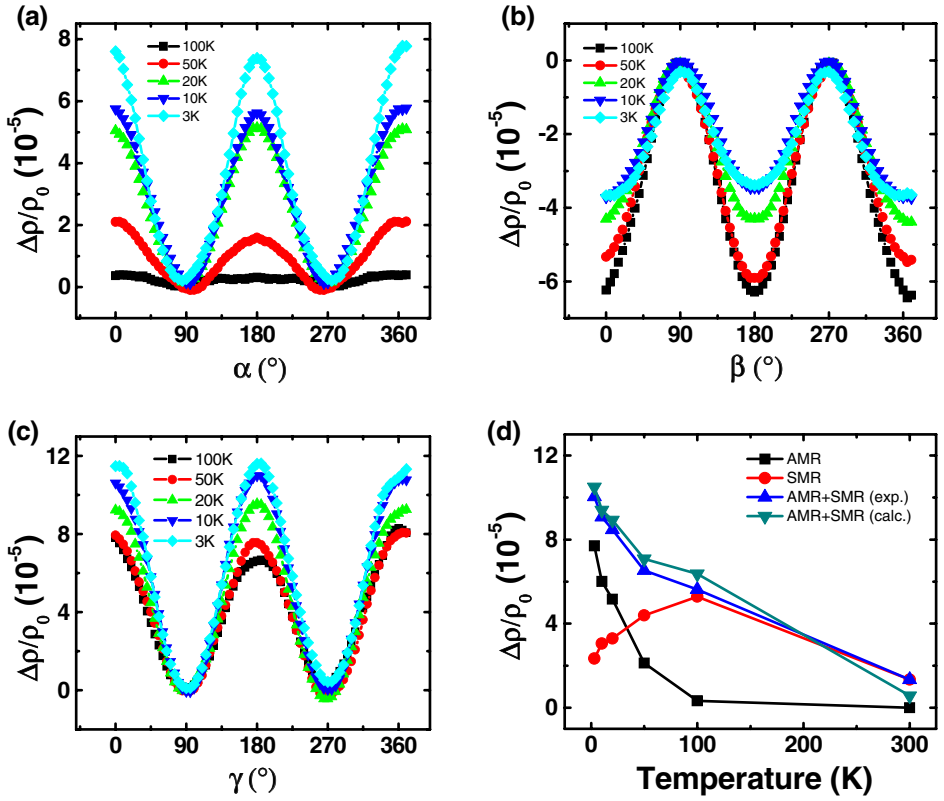

FIG. 3 (color online). Magnetoresistance data for Pd(2 nm)-YIG(30 nm) with H = 10 kOe at different temperatures for α sweeps (a), β sweeps (b), and γ sweeps (c). (d) Temperature dependence of the magnetoresistance oscillation amplitude in all three rotational configurations. α-, β- and γ-sweeps represent AMR, SMR, and AMR + SMR, respectively. "AMR + SMR (exp.)" is the amplitude of the magnetoresistance oscillations measured in the γ sweep, and "AMR + SMR (calc.)" is the sum of two amplitudes in the α and β sweeps.

$d/\lambda \sim 0.8$ according to Eq. (2), as shown in the inset of Fig. 4. Although the actual position of the peak may not exactly coincide at this value, a peak in SMR is expected to appear at $d \sim \lambda$ from the following general argument. If the spin diffusion length is much smaller than the film thickness, SMR obviously vanishes. On the other hand, if the spin diffusion length is much greater than the film thickness, then the chemical potential difference between spin-up and -down channels does not vary much across the film thickness, which consequently results in a small spin current and SMR. AMR, on contrary, is expected to increase at low temperatures as discussed earlier. Therefore, the characteristic temperature dependence provides us an important criterion to distinguish SMR from AMR. To demonstrate the thickness effect, we have prepared samples with three different Pd thicknesses: 2, 3, and 4 nm, on YIG films grown nominally under the same conditions. The results are displayed in Fig. 4. Clearly, the SMR peak position (~100 K) of the 2 nm sample agrees with the data shown in Fig. 3 from the other 2 nm sample. Using the SMR theory prediction, we can estimate the spin diffusion length of Pd at 100 K by $\lambda = 1.25d$, which yields $\lambda \sim 2.5$ nm. We note that the detailed peak width differs, which is likely due to the inevitable roughness of Pd. The SMR of the 3 nm sample also shows a well-defined peak that is located at a lower temperature (~50 K). This trend is in qualitative agreement with the SMR theory, and it implies that λ is increased to ~3.8 nm at 50 K. For the

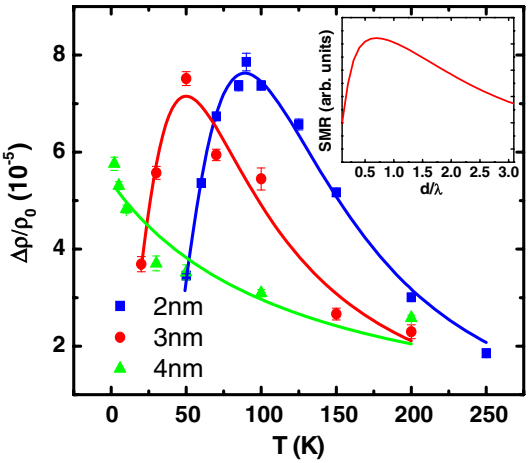

FIG. 4 (color online). SMR measured in the β sweeps as a function of temperatures for three different Pd layer thicknesses: 2, 3, and 4 nm. Inset: SMR vs d/λ calculated using Eq. (2).

4 nm sample, the peak is not captured in the temperature window of our experiments (2 to 300 K). However, the trend for the SMR peak position is in good agreement with the theoretical prediction. We note that the previously determined λ value spreads from 2 to 9 nm at room temperature [17–19] and is as large as 25 nm at 4.2 K [20]. The discrepancy may arise from the differences in the measurement techniques or in sample conditions.

Unlike SMR, the AMR magnitude is larger at lower temperatures in all samples, which confirms different physical mechanisms behind these two effects. The fact that AMR exists at low temperatures implies the existence of proximity induced ferromagnetism in Pd near the interface.

In summary, by lowering the temperature, we observe an enhanced AMR as a result of suppressed spin-flip scattering. In the meantime, SMR shows a peak, which is consistent with the SMR theory. Our results further indicate that both the magnetic proximity effect and the spin current effect coexist in Pd-YIG bilayers systems.

We would like to thank R. Shindou, B. Youngblood, I. Krivorotov, G. Bauer, and W. Beyermann for many useful discussions, and Z. Y. Wang, Z. L. Jiang, N. Amos, and J. Butler for their technical assistance. C. T. and J. S. were supported by DOE/BES Award No. DE-FG02-07ER46351, H. M. A. was supported by NSF/ECCS, and T. L. was supported by DMEA/CNN.

[1] B. Heinrich, C. Burrowes, E. Montoya, B. Kardasz, E. Girt, Y-Y. Song, Y. Sun, and M. Wu, Phys. Rev. Lett. **107**, 066604 (2011).
[2] C. Burrowes, B. Heinrich, B. Kardasz, E. A. Montoya, E. Girt, Y. Sun, Y-Y. Song, and M. Wu, Appl. Phys. Lett. **100**, 092403 (2012).
[3] S. M. Rezende, R. L. Rodriguez-Suarez, M. M. Soares, L. H. Vilela-Leao, D. Ley Dominguez, and A. Azevedo, Appl. Phys. Lett. **102**, 012402 (2013).
[4] K. Uchida, S. Takahashi, K. Harii, J. Ieda, W. Koshibae, K. Ando, S. Maekawa, and E. Saitoh, Nature (London) **455**, 778(2008).
[5] K. Uchida, J. Xiao, H. Adachi, J. Ohe, S. Takahashi, J. Ieda, T. Ota, Y. Kajiwara, H. Umezawa, H. Kawai, G. E. W. Bauer, S. Maekawa, and E. Saitoh, Nat. Mater. **9**, 894 (2010).
[6] Y.-T. Chen, S. Takahashi, H. Nakayama, M. Althammer, S. T. B. Goennenwein, E. Saitoh, and G. E. W. Bauer, Phys. Rev. B **87**, 144411 (2013).
[7] H. Nakayama, M. Althammer, Y.-T. Chen, K. Uchida, Y. Kajiwara, D. Kikuchi, T. Ohtani, S. Geprägs, M. Opel, S. Takahashi, R. Gross, G. E. W. Bauer, S. T. B. Goennenwein, and E. Saitoh, Phys. Rev. Lett. **110**, 206601 (2013).
[8] C. Hahn, G. de Loubens, O. Klein, M. Viret, V. V. Naletov, and J. Ben Youssef, Phys. Rev. B **87**, 174417 (2013).
[9] T. R. McGuire and R. I. Potter, IEEE Trans. Magn. **11**, 1018 (1975).
[10] S. Y. Huang, X. Fan, D. Qu, Y. P. Chen, W. G. Wang, J. Wu, T. Y. Chen, J. Q. Xiao, and C. L. Chien, Phys. Rev. Lett. **109**, 107204 (2012).
[11] Y. M. Lu, Y. Choi, C. M. Ortega, X. M. Cheng, J. W. Cai, S. Y. Huang, L. Sun, and C. L. Chien, Phys. Rev. Lett. **110**, 147207 (2013).
[12] Y. M. Lu, J. W. Cai, S. Y. Huang, D. Qu, B. F. Miao, and C. L. Chien, Phys. Rev. B **87**, 220409 (2013).
[13] E. Stoner, Proc. R. Soc. A **154**, 656 (1936).
[14] L. Liu, R. A. Buhrman, and D. C. Ralph, arXiv:1111.3702v3.
[15] M. Althammer, S. Meyer, H. Nakayama, M. Schreier, S. Altmannshofer, M. Weiler, H. Huebl, S. Geprägs, M. Opel, R. Gross, D. Meier, C. Klewe, T. Kuschel, J.-M. Schmalhorst, G. Reiss, L. Shen, A. Gupta, Y.-T. Chen, G. E. W. Bauer, E. Saitoh, and S. T. B. Goennenwein, Phys. Rev. B **87**, 224401 (2013).
[16] T. Lin, C. Tang, and J. Shi, Appl. Phys. Lett. **103**, 132407 (2013).
[17] K. Kondo, H. Sukegawa, S. Mitani, K. Tsukagoshi, and S. Kasai, Appl. Phys. Express **5**, 073002 (2012).
[18] V. Vlaminck, J. E. Pearson, S. D. Bader, and A. Hoffmann, Phys. Rev. B **88**, 064414 (2013).
[19] J. Foros, G. Woltersdorf, B. Heinrich, and A. Brataas, J. Appl. Phys. **97**, 10A714 (2005).
[20] H. Kurt, R. Loloee, K. Eid, W. P. Pratt, Jr. and J. Bass, Appl. Phys. Lett. **81**, 4787 (2002).